

## $H\alpha$ Distances to the Leading Arm of the Magellanic Stream

Jacqueline Antwi-Danso<sup>1,2,3</sup>, Kathleen A. Barger<sup>3,4</sup>, and L. Matthew Haffner<sup>5,6,7</sup> George P. and Cynthia Woods Mitchell Institute for Fundamental Physics and Astronomy, Texas A&M University, College Station, TX 78743, USA jadanso@tamu.edu

<sup>2</sup> Department of Physics and Astronomy, Texas A&M University, 4242 TAMU, College Station, TX 78743, USA Department of Physics & Astronomy, Texas Christian University, Fort Worth, TX 76129, USA Department of Physics, University of Notre Dame, Notre Dame, IN 46556, USA Embry-Riddle Aeronautical University, Daytona Beach, FL 32114, USA Space Science Institute, Boulder, CO 80301, USA <sup>7</sup> Department of Astronomy, University of Wisconsin-Madison, Madison, WI 53706, USA Received 2019 April 30; revised 2020 January 19; accepted 2020 January 21; published 2020 March 17

#### Abstract

The Leading Arm (LA) is a tidal feature that is in front of the Magellanic Clouds (MCs) on their orbit through the Galaxy's halo. Many physical properties of the LA, such as its mass and size, are poorly constrained because it has few distance measurements. While H $\alpha$  measurements have been used to estimate the distances to halo clouds, many studies have been unsuccessful in detecting H $\alpha$  from the LA. In this study, we explore a group of H I clouds which lie 75°-90° from the MCs. Through ultraviolet and 21 cm radio spectroscopy, this region, dubbed the LA Extension, was found to have chemical and kinematic similarities to the LA. Using the Wisconsin H $\alpha$  Mapper, we detect  $H\alpha$  emission in four out of seven of our targets. Assuming that this region is predominantly photoionized, we use a radiation model that incorporates the contributions of the Galaxy, MCs, and the extragalactic background at z=0 to derive a heliocentric distance of  $d_{\odot} \geqslant 13.4\,$  kpc. We also use this model to rederive H $\alpha$  distances of  $d_{\odot} \geqslant 5.0$  kpc and  $d_{\odot} \geqslant 22.9$  kpc to two clouds in the literature that might also be associated with the LA. Using these new measurements, and others in the literature, we provide a general trend of the variation of LA heliocentric distance as a function of Magellanic Stream longitude, and explore its implications for the origin and closest point of approach of the LA.

Unified Astronomy Thesaurus concepts: Dwarf galaxies (416); Galaxies (573); Milky Way evolution (1052); Highvelocity clouds (735); Magellanic Stream (991)

#### 1. Introduction

The Milky Way's (MWs) circumgalactic medium contains numerous high-velocity clouds (HVCs). These have various origins, including aggregates of neutral and ionized hydrogen from satellite galaxies, gas cooling out of the intergalactic medium, and Galactic fountains. As suggested by stellar chemical evolution models of the MW (e.g., Chiappini 2008), some HVCs serve as a source of low metallicity gas on which the Galaxy sustains its star formation. Therefore, a key component of understanding the relationship between baryonic feedback processes and the Galaxy's evolution relies on accurate measurements of HVC physical properties. HVC distances are especially important for estimating their basic physical properties, because many of them scale directly with distance (d). For example, their mass, size, pressure, and density scale as  $M_{\rm cloud} \propto d^2$ ,  $D_{\rm cloud} \propto d$ ,  $P_{\rm cloud} \propto d^{-1}$ , and  $n_{\rm cloud} \propto d^{-1}$ , respectively.

Spanning about 11,000 square degrees in both ionized and neutral gas (Fox et al. 2014), the gaseous streams of the interacting Magellanic Clouds (MCs)-known as the Magellanic System (MSys; see D'Onghia & Fox 2016 for a review) —are the largest collection of HVCs surrounding the MW. The MSys extends over 200° across the sky, and is comprised of the trailing Stream, the Bridge that connects the Large and Small Magellanic Clouds (LMC and SMC), and the Leading Arm (LA). As its name implies, the LA is the gaseous counterpart to the Stream that leads the MCs on their orbit through the Galactic potential.

The LA covers approximately  $60^{\circ} \times 80^{\circ}$  on the sky (Fox et al. 2018) and is separated into four main complexes

named LA I-IV. It has a complicated velocity structure with local standard of rest (LSR) velocities<sup>8</sup>  $+70 \lesssim v_{LSR} \lesssim +500$  km s<sup>-1</sup> (Wakker & van Woerden 1991; Brüns et al. 2005; Richter et al. 2017; Fox et al. 2018). This fragmented structure has been studied extensively in H I 21 cm emission (Putman et al. 1998, 2002, 2003; Brüns et al. 2005; Mcclure-Griffiths et al. 2008; Nidever et al. 2008, 2010; McClure-Griffiths et al. 2010; Venzmer et al. 2012; For et al. 2013, 2016, among others) and UV absorption (Lu et al. 1994, 1998; Sembach et al. 2001; Fox et al. 2014, 2018; Richter et al. 2018). These four complexes are accompanied by less-studied, smaller clouds that are moving at similar velocities along the same orbital path (Figure 1). Because of its complicated structure, determining the total mass of the LA requires distance estimates at multiple locations and along the full extent of the LA. These distances provide important observational constraints for modeling the interactions of the MCs and their passage through the MW's halo (Besla et al. 2007, 2010, 2012; Diaz & Bekki 2011; Guglielmo et al. 2014; Pardy et al. 2018).

One can determine HVC distances using direct or indirect methods. Previous LA studies have employed both. The former approach involves finding the distance to stars formed in situ, or bracketing the distance to the HVC by measuring absorption (or the lack of) at the velocities of the HVC in the spectra of stars whose distances are known (using them as background targets). Smoker et al. (2011) found a lack of interstellar

Throughout this study, we use the kinematic definition of the LSR, where the solar motion is 20 km s<sup>-1</sup> toward  $(\alpha, \delta)_{J2000} = (18^{h}3^{m}50^{s}29, 30^{\circ}00'16''8)$ .

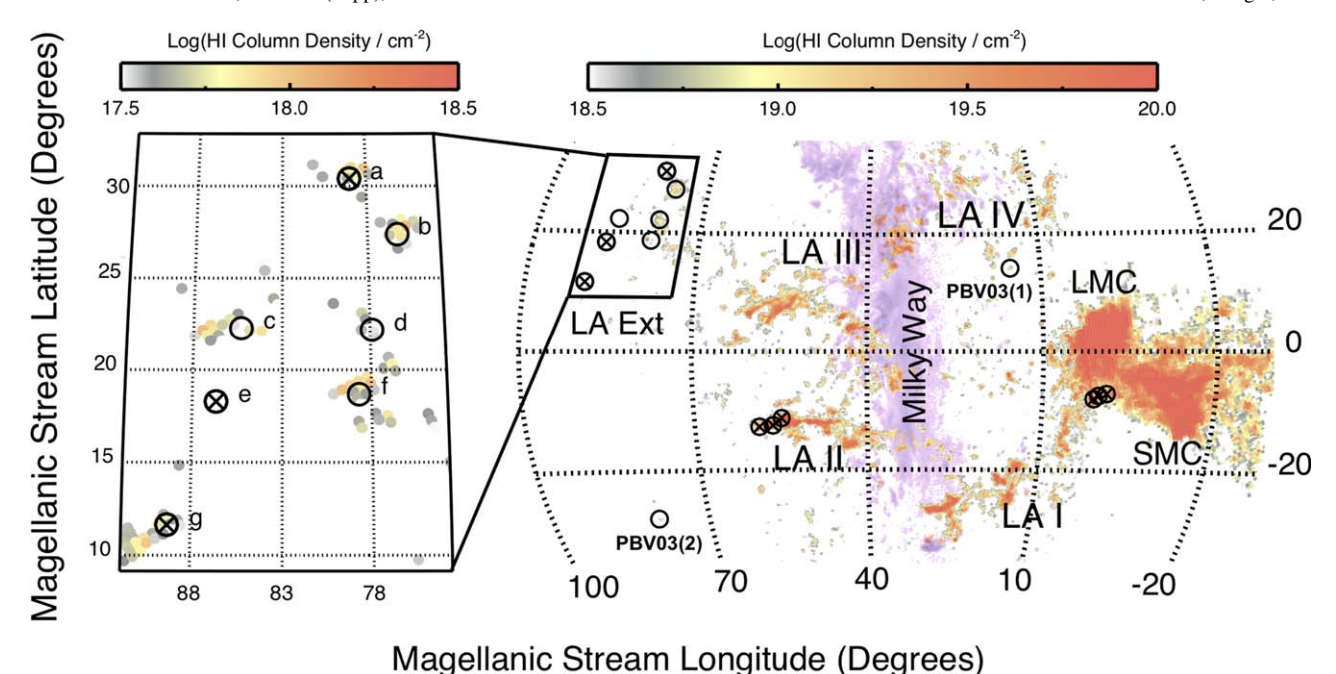


Figure 1. H I emission map of the LA and MCs in Magellanic Stream coordinates. The locations of our H $\alpha$  observations are labeled (a)–(g) in the zoomed-in region. This is shown against a backdrop of the Leiden/Argentine/Bonn (LAB) H I survey column densities from the Gaussian decompositions of Nidever et al. (2008). The open circles indicate detections and cross-filled circles nondetections. The H $\alpha$  detections labeled PBV03(1) and PBV03(2) are the (Putman et al. 2003) detections toward CHVC+266.0–8.7+336 and HVC+310.5+44.2+187, respectively. The nondetections in LA II and the outskirts of the LMC are from McClure-Griffiths et al. (2010). The global H I distribution map on the right-hand side shows Galactic All-Sky Survey (GASS) observations that have been integrated over +150  $\lesssim v_{\rm LSR} \lesssim +350 \, {\rm km \, s^{-1}}$  (McClure-Griffiths et al. 2009). The H I emission from the MW is shown in purple to distinguish it from the Magellanic emission.

absorption at high velocities toward the star HD 86248, which gives a lower distance limit to LAI (formerly called Complex EP) of  $d_{\odot} \geqslant 5.9\,$  kpc. Also in the direction of LA I, Casetti-Dinescu et al. (2014) identified a group of young stars at  $12 \leqslant d_{\odot} \leqslant 21$  kpc. They were originally thought to have formed within the LA, and therefore their distance would have been a direct distance measurement to the LA. However, Zhang et al. (2019) recently used Gaia proper motion measurements of these stars to show that they are moving with the disk of the MW and are therefore not associated with the LA. On the other hand, Fox et al. (2018) used one of these stars, CD14-A05, as a background target and found absorption at LA velocities in its spectrum. Using Gaia DR2 parallaxes and high-resolution MIKE spectra, Zhang et al. (2019) found that this star is at  $d_{\odot} = 22.0 \pm 3.0$  kpc, which places a  $1\sigma$  upper distance limit on the absorbing material of LA I at  $d_{\odot} \lesssim 25$  kpc. More recently, Price-Whelan et al. (2019) used Gaia astrometry and DECam optical images to isolate a low metallicity ([Fe/H]  $\approx -1.1$ ) young stellar group in the direction of LA II. This chemical composition is consistent with chemical abundances found by Fox et al. (2018) and Richter et al. (2018) for the LA. Price-Whelan et al. (2019) found a distance of  $d_{\odot}=28.9\pm0.1\,$  kpc to the stellar association in LA II.

One can also use models constrained by observations to indirectly estimate distances to HVCs. Using H I observations taken with the Australia Telescope Compact Array, Mcclure-Griffiths et al. (2008) showed evidence of an interaction between the LA I cloud HVC 306-2+230 and the Galactic disk. The interaction with neutral gas at Galactic velocities places the high latitude tip of LA I at a heliocentric distance of  $d_{\odot}=21\pm4.2$  kpc. By estimating the minimum travel time for the LA I complex from the LMC assuming the LA is viewed nearly face-on, Venzmer et al. (2012) estimated a distance of  $d_{\odot}\approx23.5$  kpc to LA I, which is consistent with

Mcclure-Griffiths et al. (2008). Using this same technique, Venzmer et al. (2012) estimated that LA IV lies at  $d_{\odot} \approx 74$  kpc.

The  $H\alpha$  recombination line can be used to estimate HVC distances using a three-dimensional model of the Galactic Lyman continuum flux  $(\phi_{\rm LyC})$  if one assumes that photoionization is the dominant source of ionization. Putman et al. (2003) detected  $H\alpha$  toward CHVC 266.0–18.7+336 in LA IV and HVC 310.5+44.2+187, which is located on the outskirts of LA II (Figure 1). They used these  $H\alpha$  emission-line observations and the Bland-Hawthorn & Maloney (1999, 2001) model of the Galactic ionizing radiation to derive distances of  $1.2 \le d_{\odot} \le 6.1$  kpc and  $0.4 \le d_{\odot} \le 27.5$  kpc, respectively, to these HVCs. Putman et al. (2003) is the only study to do this successfully to date, as the LA is notoriously faint in  $H\alpha$ . Rather,  $H\alpha$  nondetections have been reported along the LA, even using deep  $H\alpha$  spectroscopic surveys (Putman et al. 2003; McClure-Griffiths et al. 2010).

In this paper, we present seven new targeted H $\alpha$  pointings toward six small clouds positioned 75°-90° from the LMC (Figure 1). Fox et al. (2018) explored the O/H abundances of these clouds using Hubble Space Telescope/Cosmic Origins Spectrograph (HST/COS) absorption-line spectroscopy toward background quasars and found that the clouds are likely members of the LA based on their composition, position, and velocity. Since these clouds are leading the LA III complex by roughly 15°-30°, they might represent a diffuse leading edge of the complex. Fox et al. (2018) named this region the LA Extension (LA Ext) because it comprises smaller HI clouds located to the north of the main LA complexes. We compare our observations with the HST/COS absorption-line observations of Fox et al. (2014, 2018) to investigate the ionization conditions of this gas in Section 4. In Section 5, we use models of the ionizing radiation from the MW (Fox et al. 2014), MCs

(Barger et al. 2013), and EGB (Weymann et al. 2001) to constrain the distances of these clouds and rederive the distances to CHVC+266.0–18.7+336 and HVC+310.5+44.2 +187, which were previously detected in H $\alpha$  by Putman et al. (2003) and McClure-Griffiths et al. (2010), respectively. Finally in Section 6, we explore the implications of the trend in distance to the LA on issues that are still under debate, namely the origin of the LA, and its point of closest approach.

#### 2. Observations and Reduction

### 2.1. Sample

In the spring of 2014, we observed the LA Ext in H $\alpha$  along seven sightlines with the Wisconsin H $\alpha$  Mapper (WHAM) at the Cerro-Tololo Inter-American Observatory in La Serena, Chile. The positions of our observations, sightlines (a)– (g), are shown in the H I map in Figure 1. Our H $\alpha$  observations span a Galactic longitude (l), Galactic latitude (b), and LSR velocity range of  $(l, b, v_{LSR}) = (234^{\circ}.1, 33^{\circ}.5, +50 \text{ km s}^{-1})$  to  $(248^{\circ}.9, -1)$  $51^{\circ}6$ ,  $+250 \,\mathrm{km \ s^{-1}}$ ). In Figure 1 and Table 1, we also give the positions of our observations in the Magellanic Stream coordinate system, which has  $l_{\rm MS}=0^{\circ}$  at the center of the LMC and the  $b_{\rm MS}=0^{\circ}$  line bisecting the Stream (Nidever et al. 2008). The Magellanic Stream coordinate system is useful because it eliminates the strong distortions of the MSys in standard equatorial and Galactic coordinates. In this coordinate system, our observations span  $(l_{MS}, b_{MS}) = (76^{\circ}.3, 11^{\circ}.6)$  to (89°3, 30°5). In this region, we specifically targeted six H I cloudlets and one location off the H I emission (see Figure 1). Three of these observations were intentionally aligned with UV bright background QSOs that were used in the Fox et al. (2014, 2018) UV absorption-line studies that explored the physical and chemical properties of this gas. These include sightlines (c), (d), and (e), which overlap with their HE 1003 +0149, IRASF 09539-0439, and LBQS 1019+0147 sightlines, respectively.

## 2.2. Observations

The  $H\alpha$  emission from the LA is extremely faint and has previously been detected along only two sightlines (see Table 1), but even those detections were not along the main complexes, LA I-IV (see Figure 1). The WHAM instrument was designed to observe faint ( $I_{H\alpha} \ge 0.03 \text{ R}^9$ ) optical emission from diffuse gas in the Galactic disk and halo. With its dual-etalon Fabry-Pérot optics, combined with a 0.6 m objective lens, WHAM achieves a 1° angular resolution and 12 km s<sup>-1</sup> velocity resolution ( $R \approx 25,000$ ) over a 200 km s<sup>-1</sup> window near  $H\alpha$  (Tufte 1997; Reynolds et al. 1998; Haffner et al. 2003).

We observed the LA Ext over the course of three nights in 2014. On April 4th, we observed over a fixed geocentric (GEO) velocity range of  $+100 \leqslant \nu_{\rm GEO} \leqslant +300~{\rm km~s^{-1}}$ , corresponding to  $+65 \lesssim \nu_{\rm LSR} \lesssim +265~{\rm km~s^{-1}}$ . On May 26th and 27th, we observed over a fixed  $+60 \leqslant \nu_{\rm GEO} \leqslant +260~{\rm km~s^{-1}}$  velocity range, corresponding to  $+20 \lesssim \nu_{\rm LSR} \lesssim +220~{\rm km~s^{-1}}$ . The combined observations span  $+20 \leqslant \nu_{\rm LSR} \leqslant +265~{\rm km~s^{-1}}$ . In Figure 2, we only include the emission above  $\nu_{\rm LSR} \geqslant +35~{\rm km~s^{-1}}$  as the MW's emission is prominent at lower velocities

Each of our sightlines was observed for a total integrated exposure time of 15–19 minutes. The "on-target" and the paired "off-target" observations were each taken over a 60 s duration such that one "on-off" pair consisted of 120 s of exposure time. The off-target observations were all positioned within 12° of the on-target observations, at least 5° from the  $\log(\mathrm{H~i/cm^{-2}})=18.7$  emission, and at least 0°.55 away from bright foreground stars ( $m_{\rm V}<6$  mag). We subtracted the off-target observations from the on-target ones to remove the atmospheric contribution from our spectra.

## 2.2.1. Data Reduction, Velocity Calibration, and Extinction Correction

We reduced our H $\alpha$  data with the standard WHAM pipeline for bias subtraction, flat-fielding, ring-summing, and cosmic-ray contamination removal (see Haffner et al. 2003 for more details). Our reduced observations have an overall H $\alpha$  sensitivity of  $I_{\text{H}\alpha} \approx 30$  mR, assuming a  $30 \, \text{km s}^{-1}$  line width as measured in the simplest, resolved intermediate-velocity cloud (IVC) and HVC H $\alpha$  profiles (e.g., Tufte et al. 1998; Putman et al. 2003; Barger et al. 2012, 2017).

We used the velocity calibration and atmospheric line subtraction process described in Barger et al. (2017) and the extinction correction procedure described in Barger et al. (2013, 2017), which is briefly summarized below. The LA's complex velocity field is well mapped out along its H I 21 cm emission (e.g., Nidever et al. 2008). Using this as a guide, we centered the velocity window of our observations on the H I emission by "tuning" the pressure of the SF<sub>6</sub> gas between the etalons, since the linear relationship between SF6 pressure and wavelength has been well calibrated for WHAM (Tufte 1997).

The geocentric velocities of the gas were calibrated by converting the monitored etalon gas pressures to wavelengths using this linear relationship and then measuring their Doppler shifts relative to  $\lambda_{\text{H}\alpha} = 6562.8 \text{ Å}$ . The calibration technique we employed is essentially the reverse of the tuning process that is described in Haffner et al. (2003) and is the same velocity calibration technique that was employed by Barger et al. (2017) for WHAM H $\alpha$  observations along the Magellanic Stream. We used this technique because our observations did not cover a wide enough velocity window to include the peak of a bright atmospheric line positioned at a known geocentric velocity, which includes the OH atmospheric line centered at  $v_{\text{GEO}} =$ +272.44 km s<sup>-1</sup>. Velocities calibrated in this study are accurate to  $v_{\rm GEO} \lesssim 5~{\rm km~s^{-1}}$  (Madsen 2004) as they were all taken with the same tune. <sup>10</sup> We account for this systematic uncertainty by adding 5 km s<sup>-1</sup> in quadrature to the uncertainties of our line positions, i.e.,  $\sigma_{\text{total}, \text{H}\alpha} = \sqrt{\sigma_{\text{fit}}^2 + (5 \text{ km s}^{-1})^2}$ . These calibrated geocentric velocities were converted to the LSR frame by adding a constant velocity offset value.

We corrected our  $H\alpha$  intensities for dust extinction associated with the Galactic interstellar dust along our sightlines, but not for self-extinction. Because the LA Ext gas is diffuse, accounting for self-extinction will not change our H I column density estimates appreciably. Barger et al. (2013) found an average extinction of 1.5% for the Magellanic Bridge (see their Table 2), where the average H I column density is an order of magnitude higher than that of the LA Ext. By

 $<sup>\</sup>overline{^9}$  1 Rayleigh =  $10^6/4\pi$  photons cm $^{-2}$  sr $^{-1}$  s $^{-1}$ , which corresponds to  $I_{\rm H\alpha}=2.41\times 10^{-7}$  erg cm $^{-2}$  sr $^{-1}$ . To convert H $\alpha$  intensities to emission measures, 1 R = 2.75 ( $T_e/10^4$  K) $^{0.924}$  cm $^6$  pc, where  $T_e$  is the electron temperature (Barger et al. 2017).

 $<sup>\</sup>overline{^{10}}$  WHAM observations that are taken with different pressures, but the same interference order, will agree within  $\nu_{\rm radial} \lesssim 0.1~{\rm km\,s^{-1}}$  of each other (Barger et al. 2017).

ID	Coordinates		m Hlpha					H I <sup>d</sup>				Distance
	l, b (°)	$l_{\mathrm{MS}}, b_{\mathrm{MS}}^{\mathrm{a}}$	$I_{\mathrm{H}\alpha}^{}}^{}}$ (mR)	$f_{\text{ext,corr}}^{\text{c}}$ (%)	$(\text{km s}^{-1})$	FWHM (km s <sup>-1</sup> )	$\tilde{\chi}^2_{\rm min}$	$\log (N_{\rm HI}/{\rm cm}^{-2})$	$(\text{km s}^{-1})$	FWHM (km s <sup>-1</sup> )	${ ilde \chi}^2_{ m min}$	$d_{\odot}$ (kpc)
a	234.1, 33.5	79.0, 30.5	<47 <sup>e</sup>	5.6	•••	•••		$19.24 \pm 0.01$	$126.1 \pm 0.9$	$40.6 \pm 0.8$	1.1	
b	238.7, 33.1	76.3, 27.4	$46 \pm 6^{+23}_{-21}$	6.4	$145\pm7$	$61 \pm 5$	1.3	$19.15\pm0.01$	$154.7\pm0.7$	$30.8\pm0.7$	1.1	$10.4^{+0.8}_{-0.7}  {}^{(+6.5)}_{(-2.9)}$
c	238.5, 42.8	85.3, 22.3	$40\pm10^{+15}_{-20}$	4.7	$73\pm7$	$47\pm7$	2.1	$18.88 \pm 0.03$	$64.1\pm0.8$	$22.6\pm1.4$	1.2	$17.5^{+4.9}_{-3.5}  {}^{(+8.1)}_{(-5.3)}$
	238.5, 42.8	85.3, 22.3	$31 \pm 7^{+15}_{-18}$	4.7	$112\pm7$	$45\pm13$	1.9	$19.01\pm0.02$	$111.2 \pm 1.0$	$28.2\pm1.2$	1.1	$21.3^{+4.3}_{-3.0}$ (+16.7)
d	243.3, 37.0	77.7, 22.2	$39 \pm 3^{+10}_{-9}$	5.4	$153\pm6$	$45\pm1$	1.2	$18.96 \pm 0.03$	$166.1 \pm 0.9$	$36.7\pm1.3$	1.0	$15.1^{+0.6}_{-0.5} \stackrel{(+3.7)}{_{(-2.2)}}$
e	242.2, 46.1	86.7, 18.3	<33 <sup>e</sup>	8.5				<18.9 <sup>e</sup>				
f	246.8, 39.3	78.7, 18.7	$46 \pm 4^{+15}_{-14}$	7.4	$121\pm7$	$61 \pm 3$	1.0	$19.25\pm0.01$	$126.6\pm0.7$	$42.1\pm0.8$	1.0	$13.7^{+0.8}_{-0.5}^{(+4.9)}_{(-2.5)}$
g	248.9, 51.6	89.3, 11.6	<28 <sup>e</sup>	8.4	•••	•••		$19.13 \pm 0.01$	$97.2\pm0.5$	$25.1\pm0.7$	1.1	•••
PBV03(1) <sup>f</sup>	266.0, -18.7	15.3, 14.2	136–187 <sup>g</sup>	18.0	336			19.15	336	31		5.0-5.6
PBV03(2) <sup>f</sup>	310.9, 44.4	79.6, -28.1	61–113 <sup>g</sup>	13.7	187			18.57	187	40		22.9-30.9

#### Notes.

<sup>&</sup>lt;sup>a</sup> Magellanic Stream coordinate system, defined in Nidever et al. (2008).

<sup>&</sup>lt;sup>b</sup> H $\alpha$  intensities (not extinction-corrected). These are reported as  $I_{\text{H}\alpha} \pm 1\sigma_{-\sigma_{\text{FS}}}^{+\sigma_{\text{FS}}}$ , where  $\sigma_{\text{FS}}$  is the spread accounting for fits degenerate in  $\widetilde{\chi}_{\min}^2$  due to an insufficient velocity range of the observations. This allows us to accurately anchor the continuum fit (see Section 3).

<sup>&</sup>lt;sup>c</sup> The extinction correction for  $I_{\text{H}\alpha}$  defined as  $f_{\text{ext.corr}} = (e^{A(\text{H}\alpha)/2.5} - 1) \times 100$ , where  $A(\text{H}\alpha)$  is the total extinction.

<sup>&</sup>lt;sup>d</sup> LAB H I Survey smoothed to a 1° angular resolution to match the WHAM observations.

<sup>&</sup>lt;sup>e</sup> For the H I emission, this assumes FWHM =  $3\sigma \times$  FWHM<sub>H I</sub>, where  $\sigma$  is the standard deviation of the continuum. For the Hα emission, this assumes FWHM<sub>Hα</sub> = FWHM<sub>H I</sub> when H I emission is detected or FWHM<sub>Hα</sub> =  $30 \text{ km s}^{-1}$  when it is not detected.

f The PBV03(1) and (2) sightlines probe the compact HVCs CHVC+266.0–18.7+336 and HVC+310.5+44.2+187, respectively. The Hα and H I line properties were taken directly from Putman et al. (2003). Using the Bland-Hawthorn & Maloney (1999, 2001) model of the Galactic ionizing radiation field ( $f_{\rm esc}\approx 6\%$  normal to the disk), they find PBV03(1) to be at  $1.2\leqslant d_{\odot}\leqslant 6.1$  kpc and PBV03(2) to be at  $0.4\leqslant d_{\odot}\leqslant 27.5$  kpc. g The Hα intensity is contaminated by an atmospheric line. Putman et al. (2003) estimate the error to be between 15 and 30 mR.

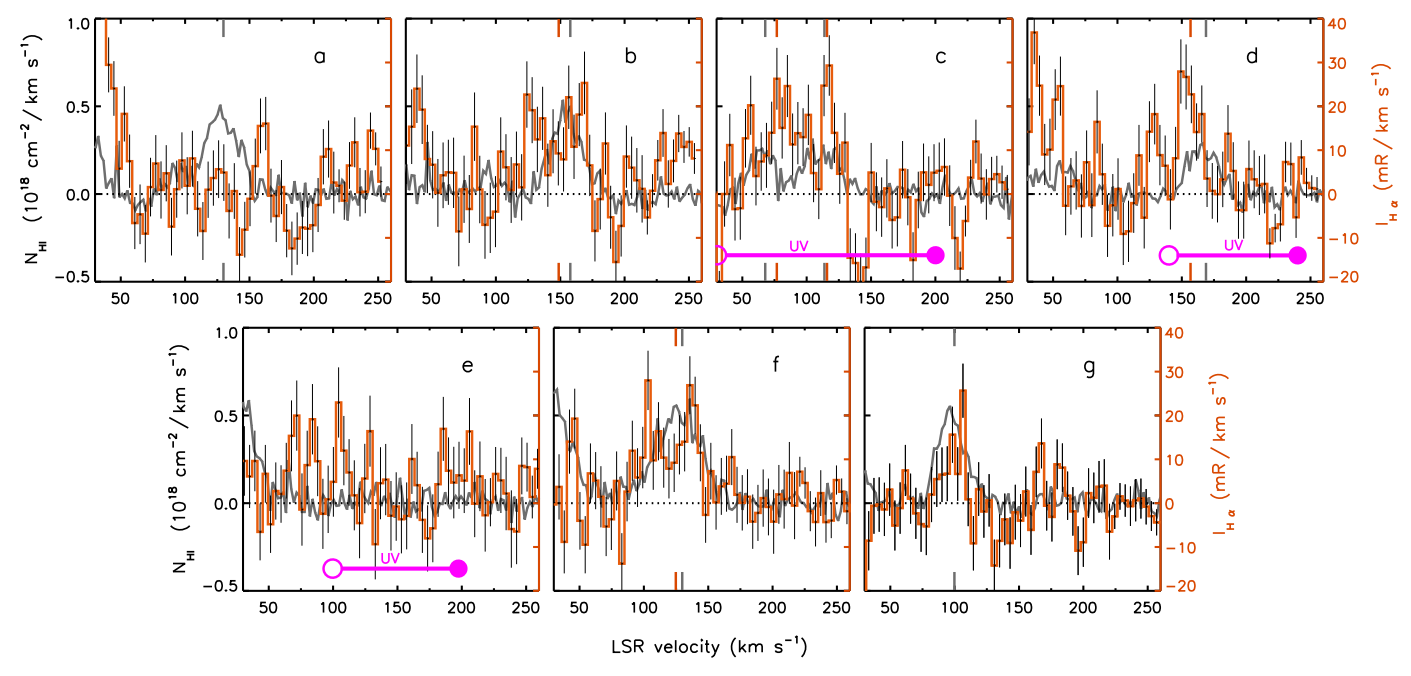


Figure 2. H I and H $\alpha$  spectra toward our sightlines plotted in gray and orange, respectively. Color-coded line markers at the top and bottom of each subplot denote the velocity centroid of each type of emission. H I, H $\alpha$ , and UV components are all detected only toward sightline (d). Si II, Si III, and Si IV absorption occurs in the  $+140 \lesssim \nu_{LSR} \lesssim +240 \,\mathrm{km \, s^{-1}}$  range, and this is shown by the pink marker. The open circle represents an upper limit on the smaller velocity as the Si II and Si III lines in (d) are blended with Milky Way absorption and saturated (see Figure 7 in Fox et al. 2014).

extension, self-extinction would increase our H $\alpha$  intensities by  $\leq 1$  mR, making its effect negligible. Using an MW dust law absorption-to-reddening ratio of the diffuse ISM of  $R_{\nu} = 3.1$  (Cardelli et al. 1989), we assume that the dust extinction is proportional to the H I emission:

$$A(H\alpha) = 5.14 \times 10^{-22} \langle N_{\rm H\,I} \rangle \text{ cm}^{-2} \text{ atoms}^{-1} \text{ mag}$$
 (1)

where  $\langle N_{H\,\text{I}} \rangle$  is the spatially averaged column density of Galactic H I along our line of sight, integrated over  $-150 \lesssim \nu_{LSR} \lesssim +150 \text{ km s}^{-1}$ . The corrected  $H\alpha$  intensity is then

$$I_{\text{H}\alpha,\text{corr}} = I_{\text{H}\alpha,\text{obs}} e^{\frac{A(\text{H}\alpha)}{2.5}}.$$
 (2)

On average, the extinction correction for the LA Ext observations is 6.7%, with a standard deviation of 1.4% (see Table 1). Such small extinction is expected, since all the sightlines are at  $b \geqslant 30^{\circ}$  above the Galactic equator. We apply this correction to our  $H\alpha$  intensities prior to our analysis in Sections 4 and 5. The uncertainty in the extinction, determined by calculating  $I_{H\alpha}$  with  $\tilde{\chi}^2 \leqslant 1.1 \tilde{\chi}^2_{\min}$  for each sightline (Section 3), is 0.5%. We do not propagate this uncertainty when determining the  $I_{H\alpha} \rightarrow \phi_{LyC}$  distances (Section 5), because it is small compared to the uncertainties from the spectral fitting and the radiation model.

## 3. Data Analysis

To explore the properties of the neutral and ionized gas phases in the LA Ext, we compare our  $H\alpha$  observations with archival H I 21 cm observations from the LAB survey (Kalberla et al. 2005) and the UV absorption-line results from Fox et al. (2018). Although higher resolution data from the Effelsberg–Bonn H I Survey is available (Winkel et al. 2016), LAB's 0.6 beam size is a closer match to WHAM's 1° beam.

The H $\alpha$  and HI spectra for our seven targeted observations, sightlines (a)– (g), are shown in Figure 2.

The LA Ext  $H\alpha$  and HI emission were modeled as a Gaussian that was combined with a linear fit to describe the continuum. For the  $H\alpha$  line fit, the Gaussian was also convolved with the WHAM instrument profile (see Haffner et al. 2003). For the HI emission, we converted brightness temperatures into column densities using the following relationship: 11

$$N_{\rm H\,I} = 1.82 \times 10^{18} \,\rm cm^{-2} \int_{V_{\rm min}}^{V_{\rm max}} T_B(v) \,dv.$$
 (3)

We fit the H I and H $\alpha$  data using the IDL MPFIT package (Markwardt 2009), which incorporates the Levenberg–Marquardt nonlinear least squares algorithm to minimize the reduced chi-squared ( $\tilde{\chi}^2$ ) of the fit. For all sightlines, we assumed a single Gaussian fit unless  $\tilde{\chi}^2_{\rm min}$  exceeded 2.5—an indication that the data was under-fitted—or if the H I spectrum revealed complex substructure consisting of more than one component, as in the case of sightline (c).

For the  ${\rm H}\alpha$  spectra, there was often insufficient continuum surrounding the emission line to perform the fit. This led to degeneracies in fit solutions with  ${\widetilde \chi}^2 \approx {\widetilde \chi}_{\rm min}^2$ . To account for this, we use the procedure outlined in Barger et al. (2017): we define a second uncertainty, the "fitting spread  $(\sigma_{\rm FS})$ ," as the difference between the minimum and maximum  $I_{\rm H}\alpha$  for models with  ${\widetilde \chi}^2$  within 10% of  ${\widetilde \chi}_{\rm min}^2$ . Hence, the  ${\rm H}\alpha$  intensities are reported as  $I_{\rm H}\alpha \pm 1\sigma_{-\sigma_{\rm FS}}^{+\sigma_{\rm FS}}$  in Table 1. This spread was determined by doing a grid search for the continuum fit and Gaussian parameters. For instance, sightline (f) has a best-fit  ${\rm H}\alpha$  intensity of 45  $\pm$  3 mR with  ${\widetilde \chi}_{\rm min}^2 = 1.0$  and a range of

<sup>&</sup>lt;sup>11</sup> This relationship holds for self-absorption in diffuse H I clouds that have an optical depth that is less than 1 (i.e.,  $\int \tau_{\rm V, H\,I} \, d\nu < 1$ ).

intensities that satisfy  $\widetilde{\chi}^2 \leqslant 1.1 \ \widetilde{\chi}^2_{\rm min}$  between  $30 \lesssim I_{\rm H\alpha} \lesssim 59 \ \rm mR$ 

We report  $H\alpha$  and H I emission only when we detect  $I_{H\alpha}$  or  $N_{H\,I} \geqslant 3\sigma \times FWHM$ —where  $\sigma$  here is the standard deviation of the continuum. For the H I emission, we assumed a representative line width of FWHM =  $30\,\mathrm{km~s^{-1}}$  and required that the  $H\alpha$  emission has a width that is at least as wide as the H I emission or  $30\,\mathrm{km~s^{-1}}$  when H I emission is not detected (as in sightline (e)). Table 1 summarizes the best-fit H I column densities,  $H\alpha$  intensities, and their corresponding line widths and velocity centroids.

# 4. Line Strengths and Kinematics in Neutral and Ionized Phases

Multiwavelength data in the radio, optical, and UV toward the same sightline enables us to explore the multiphased nature of this gas. In this section, we first compare the emission strengths and kinematics of our  $H\alpha$  observations with those of archival H I observations. These line properties are listed in Table 1. We then compare the H I and  $H\alpha$  emission with the UV metal-line absorption along sightlines (c)–(e).

There are a number of properties worth noting about the cloudlets we observe. Some of these properties are in line with what is expected for classical Galactic HVCs, and others agree better with the line properties of disturbed systems like the Magellanic Bridge and Stream. First, from the FWHM values, we find that the H $\alpha$  emission is up to twice as broad as the 21 cm emission. Although in general, ionized gas line widths are broader than those for neutral gas, that is usually not the case in classical HVCs (e.g., Complexes M, C, and A; Tufte et al. 1998; Barger et al. 2012). The only known exception to this is Complex K (Haffner et al. 2001). Conversely, in more complex systems like the Magellanic Bridge, the H $\alpha$  line widths are noticeably larger (Barger et al. 2012). This may indicate that the H $\alpha$  emission is tracing gas that is more turbulent (see Section 2.2 in Barger et al. 2012 for a more detailed discussion of the different scenarios under which this is possible). Second, there is a significant detection of HI emission toward sightlines (a) and (g), but no H $\alpha$  emission detected at the  $3\sigma$ confidence level, although  $H\alpha$  is detected at  $2\sigma$  toward sightline (g). Third, there is no correlation between the estimated H $\alpha$  intensities and HI column densities, although the line centroids agree to within 13 km s<sup>-1</sup>. This property of our observed emission is generally in agreement with what is expected for HVCs, since HVCs tend to exhibit uncorrelated  $H\alpha$  and H I emission strengths (e.g., Tufte et al. 1998; Haffner et al. 2001; Haffner 2005, PBV03, Hill et al. 2009; Barger et al. 2012, 2013, 2017).

Fox et al. (2014) studied the UV absorption toward background QSOs in three of our sightlines. They reported no LA absorption along sightlines (c) and (e), which overlap with QSOs HE 1003 +0149 and LBQS 1019+0147, respectively. Their study focuses on the  $+200 \lesssim \nu_{\rm LSR} \lesssim +300~{\rm km~s^{-1}}$  portion of the spectra along those two particular sightlines, whereas in this study we have centered our observations at  $\nu_{\rm LSR} \approx +150~{\rm km~s^{-1}}$  based on the H I Gaussian decompositions of Nidever et al. (2008). Fox et al. (2014) focused on this higher velocity range because the absorption of the low ionization species (e.g., C II, S II, and Si II) is saturated and too blended with the MW's absorption to easily be distinguished. However, along sightline (c), there is absorption at  $+40 \lesssim \nu_{\rm LSR} \leqslant +200~{\rm km~s^{-1}}$ , where there are two H I emission lines present. Similarly, there is absorption present in these low

ionization species along sightline (e) at  $+100 \lesssim v_{LSR} \leqslant +200 \ \text{km s}^{-1}$  (see Figure 2). The asymmetric shape of the blended absorption from  $-60 \lesssim v_{LSR} \lesssim +180 \ \text{km s}^{-1}$  along sightline (c) and from  $-80 \lesssim v_{LSR} \lesssim +200 \ \text{km s}^{-1}$  along sightline (e) (sightlines HE 1003+0149 and LBQS 1019+0147 in Figure 7 of Fox et al. 2014) strongly suggests that, in addition to MW absorption, there is also absorption that is related to an MW IVC, HVC, and/or the LA Ext. The asymmetric shape of the absorption in the high-ionization species Si IV and C IV along sightline (c) suggests that this cloudlet is highly ionized. Along sightline (e), there are also weak hints of absorption in these high-ionization species.

The UV absorption along sightline (d) is also blended with the MW and hence, difficult to separate; though, Fox et al. (2014, 2018) indicated that the LA was detected in absorption along this sightline. The C II, Si II, Si III, and Si IV absorption spans  $+140 \lesssim \nu_{\rm LSR} \leqslant +240~{\rm km~s^{-1}}$ , where the lower velocity limit of the LA contribution is estimated from the wing of an H I emission line centered at  $\nu_{\rm LSR} = +166 \pm 1~{\rm km~s^{-1}}$ . We mark the kinematic extent of the absorption toward background quasar IRASF 09539-0439 in Figure 2. This absorption overlaps with both the H I and H $\alpha$  emission. The detection of high-ionization species toward sightlines (c) and (d) in addition to both H I and H $\alpha$  indicates that this cloud is multiphased and is made up of gas with an electron temperature of  $10^{3.9} \lesssim T_e \lesssim 10^{5.3}~{\rm K}$  (e.g., Gnat & Sternberg 2007; Oppenheimer & Schaye 2013).

#### 5. Distance to the LA Ext and Other LA HVCs

Because  $H\alpha$  is a recombination line, its line strength is directly proportional to the rate of ionization per surface area of the emitting gas in photoionization equilibrium conditions. Using this premise, we place constraints on the distance to the LA Ext using an equation derived in Barger et al. (2012) that relates the  $H\alpha$  intensity of a gas cloud with the source of its ionization:

$$\phi_{\rm H\,I \to H\,II} = 2.1 \times 10^5 \left( \frac{I_{\rm H\alpha}}{0.1 \,\rm R} \right) \times \left( \frac{T_e}{10^4 \,\rm K} \right)^{0.118} \text{ photons cm}^{-2} \,\rm s^{-1}.$$
 (4)

We assume that the incident ionizing flux is dominated by photons from OB stars which escape the MW's ISM and that the LA Ext cloudlets are optically thick to the Lyman continuum and optically thin to  ${\rm H}\alpha$  photons (since  $\log{(N_{\rm H\,I}/{\rm\,cm^{-2}})}\geqslant 18$ ). With this assumption,  $\phi_{\rm H\,I\to H\,II}\approx \phi_{\rm LyC}$ , where  $\phi_{\rm LyC}$  is the incident Lyman Continuum flux. We also include the small—but not negligible—ionizing contributions from the MCs and the low-redshift ( $z\approx 0$ ) extragalactic background (EGB).

We use the Fox et al. (2014) model for the combined Galactic, Magellanic, and extragalactic ionizing radiation field. This model is an updated version of the Fox et al. (2005) model, which is based on those of Bland-Hawthorn & Maloney (1999, 2001, 2002) and Barger et al. (2013). Here, the fraction of hard photons escaping normal to the disk is  $f_{\rm esc,MW} \approx 6\%$ . For the ionizing contribution of the LMC and SMC,  $f_{\rm esc,LMC} = 3 \pm 1.0\%$  and  $f_{\rm esc,SMC} = 4 \pm 1.5\%$ .

The MW, LMC, and SMC ionization models specifically predict the amount of radiation that is escaping out of the disks of these galaxies into the circumgalactic medium. To estimate

how far the ionizing radiation extends from the host galaxy disk, these flux models were calibrated using distances to HVCs and IVCs obtained via the direct methods described in Section 1. For the MW, this calibration was done using  $H\alpha$ emission-line observations of Complexes A, M, C, and K and distance measurements from absorption-line spectroscopy (see Bland-Hawthorn & Maloney 1999, 2002; Bland-Hawthorn & Putman 2004). This calibration enables one to use make reasonable estimates of HVC distances using the  $I_{
m Hlpha} 
ightarrow \phi_{
m Lyc}$ distance method (e.g., Putman et al. 2003; Barger et al. 2012, 2017). The escape fraction for the MW has a factor of 2 uncertainty, which could change the model fluxes by up to 50% Bland-Hawthorn & Maloney (2002). Although these uncertainties are large, the MW model has produced distances to the Smith Cloud (Putman et al. 2003) and Complex A (Barger et al. 2012) that are in agreement with kinematic distance estimates (Lockman et al. 2008) and stellar absorption distance brackets (Wakker et al. 1996, 2008; Ryans et al. 1997; van Woerden et al. 1999).

The LMC and SMC flux models were calibrated using  ${\rm H}\alpha$  observations of the Magellanic Bridge and the well-measured distances of the LMC and SMC (Barger et al. 2013). We include the ionizing contribution of the EGB, which is estimated to be  $\phi_{\rm LyC,EGB} \lesssim 10^4$  photons cm<sup>-2</sup> s<sup>-1</sup> at z=0 (Weymann et al. 2001), which will raise the  $I_{\rm H}\alpha$  by up to 5 mR using Equation (4). We assume that the EGB is isotropic, and given that the cloudlets are optically thin to  ${\rm H}\alpha$  and LyC photons, that the combined model is independent of observer axis (that is, it is adequate for determining the combined radiation of the MW, MCs, and EGB incident on an HVC).

We determined the ionizing flux needed to reproduce the observed H $\alpha$  intensities using Equation (4) and then used the combined model of the ionizing radiation from the MW, MCs, and EGB (Figure 4) to determine the distances of the cloudlets from the Sun. However, since there are other sources of ionization that we may not have accounted for, this approach only provides a lower distance limit. That is, if there are other sources of ionization contributing to the observed H $\alpha$  emission, the contribution from photoionization would be less, which would place the clouds at a larger distance. Other possible types of ionization occurring in the clouds include collisional ionization associated with ram pressure stripping and selfionization from a "shock cascade" created when parts of the cloud that have been stripped and decelerated by the halo collide with the other parts of the cloud (see Bland-Hawthorn et al. 2007; Tepper-García et al. 2015; Barger et al. 2017).

We quantify the effects of two sources of uncertainty on the distance to each sightline: the statistical uncertainty and the spread in intensities  $(\sigma_{FS})$  associated with degenerate fits, which have  $\widetilde{\chi}^2 \approx \widetilde{\chi}^2_{min}$  (see Section 3). We calculated the uncertainties on the LA Ext distance due to the  $1\sigma$  statistical uncertainties, as follows:

$$\sigma^{+} = d(I_{H\alpha} + 1\sigma) - d(I_{H\alpha})$$
  
$$\sigma^{-} = d(I_{H\alpha}) - d(I_{H\alpha} - 1\sigma).$$

The uncertainties on the distance due to  $\sigma_{\rm FS}$  were calculated in the same fashion. For this, we consider all fits satisfying  $\widetilde{\chi}^2_{\rm min} \leqslant \widetilde{\chi}^2 \leqslant 1.1 \widetilde{\chi}^2_{\rm min}$ . Therefore, each sightline has a distance given by  $d_{1\sigma^-}^{1\sigma^+} (+\sigma_{\rm FS})$ . For example, sightline (f) is at  $d_\odot = 13.7^{+0.8}_{-0.5}$  kpc for  $I_{\rm H\alpha} = 41 \pm 4$  mR, and its range of distances when accounting for the spread in intensities for

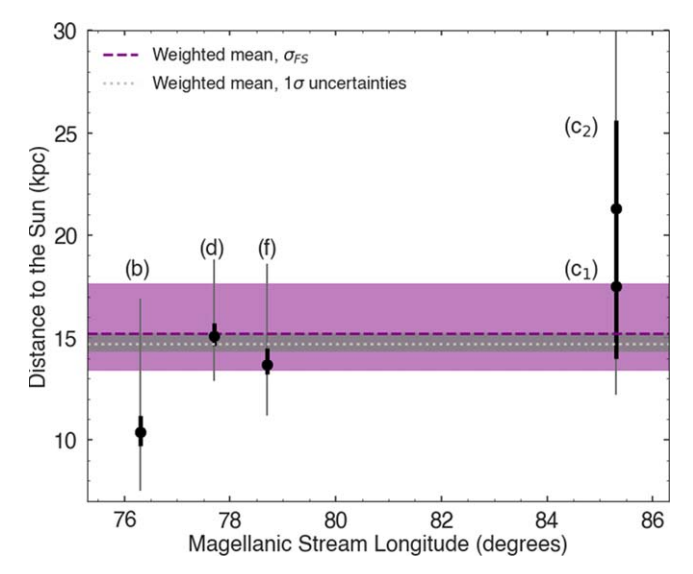


**Figure 3.** Heliocentric distances to the LA Ext cloudlets with H $\alpha$  detections as a function of Magellanic Stream longitude. We mark the statistical uncertainties with thick lines and the spread in distances from fits that have  $\widetilde{\chi}^2 \leqslant 1.1\ \widetilde{\chi}^2_{\rm min}\ (\sigma_{\rm FS})$  with thin lines. The gray and purple bands represent the uncertainties on the weighted mean distances due to the  $1\sigma$  statistical uncertainties and spread in fitted intensities, respectively.

fits degenerate in  $\tilde{\chi}^2$  is  $11.2 \leqslant d_{\odot} \leqslant 18.4$  kpc for  $31 \leqslant I_{H\alpha} \leqslant 52$  mR (see Table 1). Calculating the spread in intensities for each sightline also allows us to take into consideration variation in the  $H\alpha$  intensities of up to 50%. This way, the uncertainties in the radiation model are accounted for in our distance estimates.

Since the size of the explored LA Ext region is small compared to the size of the entire LA, we assume that all of the LA Ext cloudlets are at the same distance in order to calculate a weighted mean distance. To account for the asymmetry of the uncertainties in distance, we use the technique described in Barlow (2003). We find a weighted distance of  $d_{\odot} = 14.7^{+0.5}_{-0.4}$  kpc using the  $1\sigma$  statistical uncertainties and  $d_{\odot} = 15.2^{+2.4}_{-1.8}$  kpc using the spread in intensities from multiple fits degenerate in  $\tilde{\chi}^2$ . We show the H $\alpha$  distances for each sightline as well as the resultant weighted distances as a function of Magellanic Stream longitude in Figure 3. Because the method we employed can only be used to place a lower limit on the distance to these clouds, the LA Ext is at least 13.4 kpc from the Sun.  $^{13}$ 

In determining this lower distance limit, we treated the  ${\rm H}\alpha$  components along sightline (c) as separate sightlines, as shown in Figure 3. It is uncertain if both are actually physically associated with the LA Ext. The lower velocity H I component of sightline (c) at  $v_{\rm LSR}=+73\pm7~{\rm km~s^{-1}}$  (denoted  $c_1$  in Figure 3) is kinematically offset from the  ${\rm H}\alpha$  and H I emission features along our other sightlines by  $\Delta v_{\rm LSR}\approx-40~{\rm km~s^{-1}}$ . This deviation from the bulk motion of the LA Ext may indicate that it is a Galactic IVC. Excluding this lower velocity component of sightline (c) from our calculations increases  $d_{\odot}$  by 0.43 kpc.

<sup>12</sup> We used the Barlow (2003) Java applet found at https://www.slac.stanford.edu/~barlow/java/statistics5.html.

edu/~barlow/java/statistics5.html. <sup>13</sup> Excluding the contribution from the MCs changes the distance of the LA Ext from  $d_{\odot} \geqslant 13.4$  to  $d_{\odot} \geqslant 16.7$  kpc.

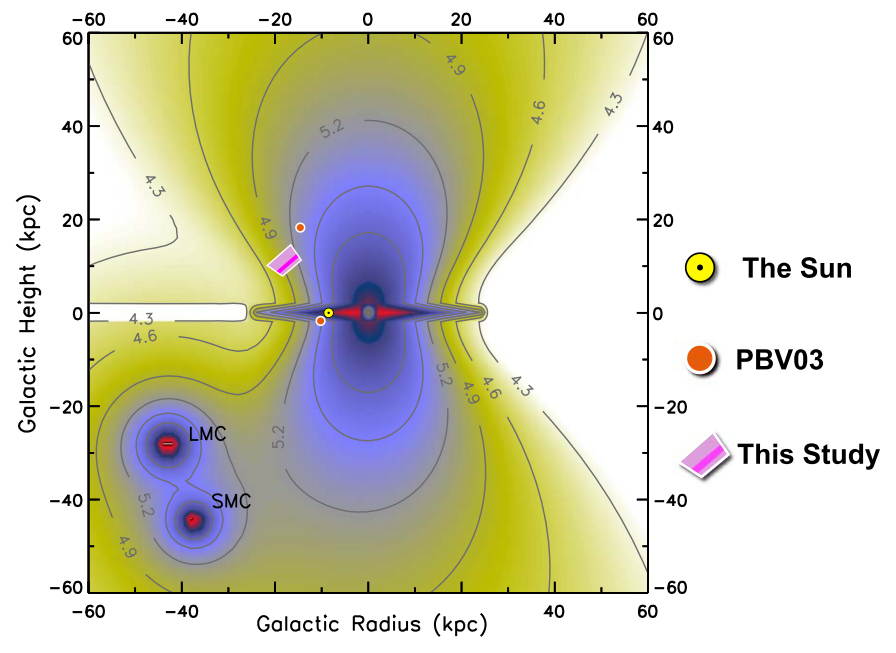


Figure 4. A  $120 \times 120$  kpc slice through the three-dimensional Lyman continuum flux model centered on the Milky Way. This radiation field includes contributions from the Milky Way (Fox et al. 2005), Magellanic Clouds (Barger et al. 2013), and extragalactic background at  $z \approx 0$  (Weymann et al. 2001). The contour lines are  $\log(\phi_{\rm LyC})$  in photons cm<sup>-2</sup> s<sup>-1</sup>. The locations in the Galactic halo at which H $\alpha$  emission was detected toward the LA Ext and the Putman et al. (2003) HVCs—CHVC +266.0–18.7+336 and HVC+310.5+44.2+187—are shown as the pink polygon and orange dots, respectively. The Sun is marked as a yellow dot for reference. Because there could be other sources of ionization besides photoionization, we consider the distances derived using this method as lower distance limits.

Additionally, it is important to note that the LA Ext overlaps with Wannier complex WB, which covers  $(l, b, \nu_{\rm LSR}) = (225^{\circ}, 0^{\circ}, +70~{\rm km~s^{-1}})$  to  $(265^{\circ}, 60^{\circ}, +170~{\rm km~s^{-1}})$  (Wannier et al. 1972; Wakker & van Woerden 1991). Using absorption-line spectroscopy toward a background star, Thom et al. (2006) placed the distance of this cloud at  $d_{\odot} \lesssim 8.8^{+2.3}_{-1.3}~{\rm kpc}$ . Therefore, based on our  ${\rm H}\alpha$  distances, the LA Ext cloudlets explored in this study are unlikely to be associated with Wannier Complex WB.

As mentioned in Section 1, prior to this study, there were only two H $\alpha$  detections in gas clouds that might be associated with the LA. These detections, which were made by Putman et al. (2003), are listed in Table 1. Using Fabry-Pérot H $\alpha$ observations from the Anglo-Australian Telescope and the Bland-Hawthorn & Maloney (1999, 2001) model for the ionizing flux from OB stars in the disk of the MW, Putman et al. (2003) derived distances to CHVC+266.0-18.7+336 and HVC+310.5+44.2+187. The former is located in the same part of the sky covered by LA IV and the latter on the outskirts of LA II (see Figure 1). We used the combined MW, MCs, and EGB flux models for the incident ionizing radiation and the Putman et al. (2003) H $\alpha$  intensities to rederive the distances to these HVCs (Table 1). We include a summary of all  $H\alpha$ distances against a slice through the radiation model in Figure 4.

## 6. Discussion

The LA is patchy and covers one-eighth of the sky ( $\sim$ 5600 square degrees). The fragmented nature of the LA and its large size present challenges to finding distances along its entire length. Nevertheless, a few studies have been able to place constraints on the distance to LA I (Putman et al. 2003; Mcclure-Griffiths et al. 2008; Venzmer et al. 2012; Zhang et al. 2019) and LA II (Smoker et al. 2011; Price-Whelan et al. 2019) using radio and optical spectroscopy, as well as optical imaging. The details and limitations of these methods are

discussed in Section 1. All LA distance measurements in the literature, with the exception of those from Mcclure-Griffiths et al. (2008), Price-Whelan et al. (2019), and the Venzmer et al. (2012) LA I estimate are either upper or lower limits due to limitations of the methods used. The distances inferred from the Putman et al. (2003)  ${\rm H}\alpha$  measurements and our LA Ext  ${\rm H}\alpha$  measurements are lower distance limits for reasons discussed in Section 5. Similarly, the distance inferred from the UV absorption observed toward background star CD14-A05 (Fox et al. 2018) at  $d_{\odot}=22\pm3\,$  kpc (Zhang et al. 2019), provides a  $1\sigma$  upper limit of  $d_{\odot}<25\,$  kpc to the absorbing gas. We have plotted all of these LA distance measurements and their  $1\sigma$  uncertainties as a function of Magellanic Stream longitude in Figure 5.

Based on predictions from the extensive suite of simulations of the dynamical history of the MCs (see D'Onghia & Fox 2016 for a review), we can assume that because LA I, II, and III are leading the orbital path of the two galaxies, and because the MCs are just past perigalacticon in their orbits, these complexes and all of their associated cloud fragments are expected to be at a distance closer than that of the Clouds. That is, the LA observations should be at a distance of  $d \lesssim 55$  kpc from the Galactic center. Venzmer et al. (2012) estimated a distance of  $d_{\odot} \approx 74$  kpc to LA IV. Based on the reasoning above; however, this distance is inconsistent with what is expected for an HVC complex that is leading the MCs. Furthermore, although there are H I studies that have suggested a kinematic association of LA IV (Venzmer et al. 2012; For et al. 2013, 2016) with the LA, no one has yet investigated the chemical abundance patterns in that region to confirm membership. This is mainly because searches for z < 1 QSOs toward LA IV clouds along sightlines with HI emission have been unsuccessful. For these reasons, we do not include the Venzmer et al. (2012) distance to LA IV in Figure 5.

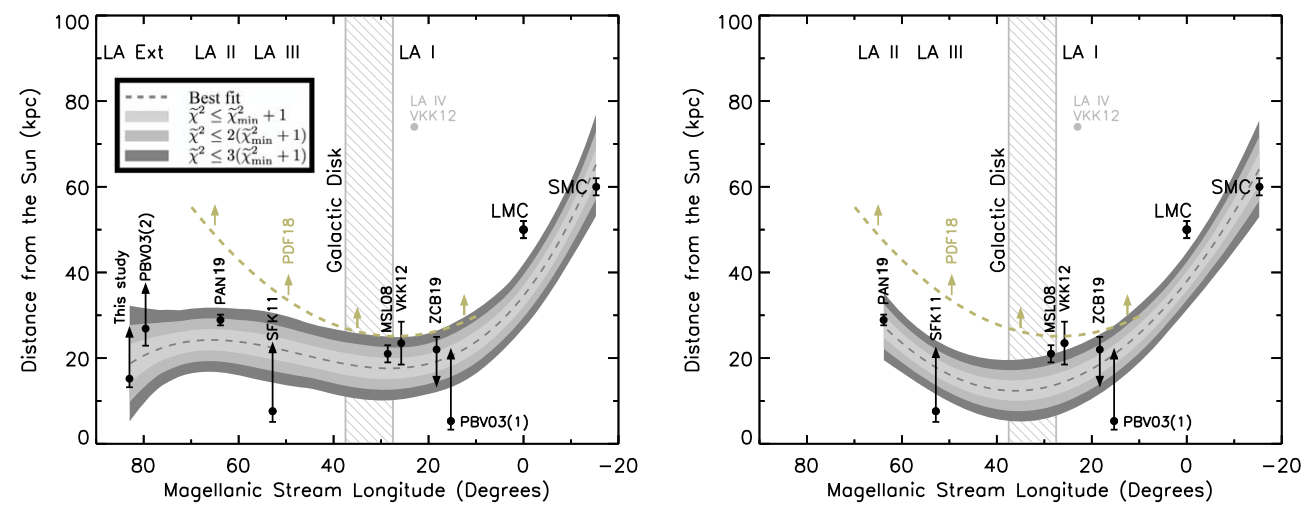


Figure 5. Compilation of all LA distance constraints and their  $1\sigma$  uncertainties. The literature distances and their corresponding abbreviations are as follows: Putman et al. (2003; PBV03), Price-Whelan et al. (2019; PAN19), Smoker et al. (2011; SFK11), Mcclure-Griffiths et al. (2008; MSL08), Venzmer et al. (2012; VKK12), and Zhang et al. (2019; ZCB19). The dashed gray line marks our best-fit distance, obtained by randomly sampling the parameter space covered by the distances and fitting polynomials of various orders to the draws (Section 6). We fixed the maximum allowable distance for each upper limit at 50 kpc, based on what simulations predict for an HVC leading the Magellanic Clouds. The light gray envelope illustrates fits that are within  $\tilde{\chi}^2 \leqslant \tilde{\chi}_{\min}^2 + 1$ , and the progressively darker envelopes are for fits with  $\tilde{\chi}^2$  values 2 and 3 times that of the light gray envelope. We also include the line-of-sight distances predicted by the Pardy et al. (2018) simulation (abbreviated PDF18) as a dashed olive green line, but we do not use them to constrain our models. Left: best-fit model including our LA Ext and HVC+310.5+44.2+187 distances. Right: best-fit model excluding the aforementioned, as they may have a non-Magellanic origin. In both cases, simulations predict higher line-of-sight distances than observed.

In simulations of the MSys, predicted heliocentric distances are often compared with measured distances as a function of longitude to judge the quality of the model(s) used. Because the LA has fewer distance estimates than the other parts of the MSys, this comparison was for a long time done using only the Mcclure-Griffiths et al. (2008) distance (Diaz & Bekki 2011; Besla et al. 2012; Guglielmo et al. 2014; Pardy et al. 2018), and more recently, the Price-Whelan et al. (2019) distance (Tepper-García et al. 2019). With the compilation of all the LA distances in the literature, in addition to our three new ones, we make this comparison along the entire length of the LA for the first time. To determine whether or not the observed trend in distance to the LA matches predictions from simulations, we produced a fit to the measured distances (Figure 5). Because we did not want to make any assumptions about the functional form of the two-dimensional structure of the LA, we fit polynomials of various orders using MPFIT to random draws from the parameter space covered by the measurements. This way, we sampled all possible fits in the distance ranges covered by the measurements and their corresponding limits and  $3\sigma$ uncertainties. The maximum allowed distance for the LA was set to 50 kpc, based on the orbit of the MCs. We would like to point out that the fit should be viewed more as an approximation and a visual aid than an exact solution. This is because we have not modeled and accounted for the non-Gaussianity in the upper and lower limits. Additionally, we are more interested in the general distance trend suggested by the fit. For this reason, we also show fits with up to  $3(\tilde{\chi}^2_{\min} + 1)$  in Figure 5. Readers interested in producing a model with a more rigorous treatment of the upper and lower limits can refer to the methodology of Isobe et al. (1986).

One thing that is evident from Figure 5 is that the distance to the LA varies from its base near the Clouds to its tip in the halo. Using the excellent spatial resolution offered by the GASS survey, For et al. (2016) reported the first observational evidence of this variation in distance. The compilation of distances to the LA in Figure 5 not only appears to lend support

to this picture, but also provides constraints that can be used to estimate the ages of the LA HVCs at those locations. Combined, ages and distances can provide strong constraints on the origin of the progenitor clouds of the LA.

The exact origin of the LA is still a subject of debate. Although the fit in Figure 5 was not fixed to either of the MCs, the best-fit line passes through the SMC and not the LMC. This is an interesting result because it is consistent with the findings of For et al. (2016), Fox et al. (2018), and Richter et al. (2018). Recent simulations suggest that the LA contains material from both the LMC and the SMC (Pardy et al. 2018). While they are able to broadly reproduce the observed velocities and positions of the HVCs belonging to the LA, they predict higher heliocentric distances than observed. Because of this, and because the LA exhibits a large spread in metallicities and ages (Fox et al. 2018), some have suggested that the LA may have multiple origins. D'Onghia & Lake (2008) proposed that the MCs could be the two largest galaxies in an accreted group of dwarfs. They estimated that 7 of the 11 brightest MW satellites may have been part of this accreted group. More recently, Koposov et al. (2015a, 2015b, 2018) and Drlica-Wagner et al. (2016) have discovered 10 ultra-faint galaxies in proximity to the MCs. In this scenario, the LA could be gaseous debris from material that was stripped from dwarf galaxies that are in front of the orbital path of the MCs (Yang et al. 2014; Hammer et al. 2015). This LA formation scenario is consistent with the variation of the chemical composition pattern that Fox et al. (2018) and Richter et al. (2018) found for LA I, II, III, and the LA Ext, and could explain why the LA lacks an extended and old tidal stellar stream. Furthermore, the only simulations that are able to reproduce LA IV are those that invoke the dwarf galaxy scenario. If it is true that some parts of the LA originated from gas-bearing dwarfs, this might explain why LA IV is extremely fragmented and why it might lie at a much higher distance than other LA complexes ( $d_{\odot} \approx 74$  kpc; Venzmer et al. 2012).

Although the metallicity of the LA Ext has been shown to be consistent with a Magellanic origin, Tepper-García et al. (2019) point out that the original chemical signature of the LA cloudlets could be washed out due to mixing. Additionally, they show that it is highly unlikely for an HVC to survive the ram pressure stripping due to the hot Galactic halo. They suggest based on this, that LA-North ( $l_{\rm MS} \lesssim 65^{\circ}$ ) would need to be protected in a deep dark matter potential, such as a dwarf galaxy, to survive those conditions. On the contrary, others have demonstrated that it is possible for a neutral hydrogen gas cloud to survive the conditions in the Galactic halo for several million years provided it is large (>250 pc), although it will end up fragmented (Armillotta et al. 2017).

If the the LA Ext and HVC+310.5+44.2+187 are part of the LA, then the line of best fit places the closest point of approach of the LA at  $d_{\odot} \approx 20\,$  kpc, and it occurs at  $l_{\rm MS} = +80^{\circ}$ . If they are not, then the minimum distance is  $d_{\odot} \approx 15$  kpc, and it occurs at  $l_{\rm MS} = +36^{\circ}$ . The position of the point of closest approach in the right panel of Figure 5 is consistent with predictions from Pardy et al. (2018); however, their minimum distance is higher. Figure 5 also demonstrates there is still much uncertainty in the distances to the LA. Many of the distance measurements are derived through indirect methods, and some are only able to provide upper or lower distance bounds. We stress that more direct distance measurements of the LA are needed to constrain the three-dimensional structure of the LA, its total mass, and the rate at which it is accreting onto the MW. Nevertheless, our compilation of LA distances to date provides important constraints that will inform future simulations of the dynamical history and orbital motion of the MCs.

## 7. Summary

In this study, we have presented WHAM observations toward seven cloudlets in the LA Ext, a region recently found by Fox et al. (2018) to be chemically consistent with the LA. Toward four out of seven of our sightlines, we detected faint H\$\alpha\$ emission with intensities  $33 \le I_{\rm H}{\alpha} \le 49$  mR at velocities  $+73 \le \nu_{\rm LSR} \le +154$  km s<sup>-1</sup> (Table 1). Three of these sightlines align with UV-bright background QSOs that were used by Fox et al. (2014, 2018) to explore this gas through absorption-line spectroscopy. The detection of H I and H\$\alpha\$ in emission as well as low and high-ionization species in absorption (C II, Si II, Si III, Si IV, and C IV) indicates that the LA Ext gas is multiphased.

We estimated the distance to the LA Ext by assuming that photoionization is the dominant ionizing mechanism and that the incident ionizing radiation field includes contributions from the Milky Way, Magellanic Clouds, and extragalactic background at  $z\sim0$ . Using this radiation model (Figure 4), we determined that the LA Ext is at a heliocentric distance of  $d_{\odot}\geqslant13.4$  kpc from the Sun. This distance places it at a height of  $|z|\gtrsim8.6$  kpc above the Galactic disk. We also rederived the H $\alpha$  distances in Putman et al. (2003) for CHVC+266.0-18.7 +336 and HVC+310.5+44.2+187 with this model and found that they are located at  $d_{\odot}\geqslant5.0$  and  $d_{\odot}\geqslant22.9$  kpc, respectively. If these two clouds are associated with the LA, then the above represent distances to LA IV and the gas on the outskirts of LA II.

Finally, we combined our estimates with distance measurements in the literature to show how the distance to the LA varies along its length (Figure 5). If HVC+310.5+44.2+187

and the LA Ext are indeed associated with the LA, then the minimum LA distance is  $d_{\odot}\approx 20$  kpc and occurs at  $l_{\rm MS}=+80^{\circ}$ .

We thank the anonymous referee for a constructive report that greatly helped to improve the quality of this paper. We are also grateful to Andrew Fox for feedback on an earlier draft, and to Josh Peek for useful conversations on the origin of the stars in LA I. WHAM operations for these observations were supported by National Science Foundation (NSF) awards AST 1108911 and AST 1714472/1715623 and AST 1940634. This paper includes archived LAB and GASS HI data obtained through the AIfA HI Surveys Data Server (https://www.astro.uni-bonn.de/hisurvey/index.php). The IDL routines are available at http://purl.com/net/mpfit. Jacqueline Antwi-Danso received additional support through NSF grant PHY-1358770 and Kat Barger through NSF Astronomy and Astrophysical Postdoctoral Fellowship award AST~1203059.

Software: MPFIT (Markwardt 2009).

Facilities: WHAM (University of Wisconsin, Madison Wisconsin H-Alpha Mapper).

#### ORCID iDs

Jacqueline Antwi-Danso https://orcid.org/0000-0002-0243-6575

Kathleen A. Barger https://orcid.org/0000-0001-5817-0932

L. Matthew Haffner https://orcid.org/0000-0002-9947-6396

## References

```
Armillotta, L., Fraternali, F., Werk, J. K., Prochaska, J. X., & Marinacci, F.
  2017, MNRAS, 470, 114
Barger, K. A., Haffner, L. M., & Bland-Hawthorn, J. 2013, ApJ, 771, 132
Barger, K. A., Haffner, L. M., Wakker, B. P., et al. 2012, ApJ, 761, 145
Barger, K. A., Madsen, G. J., Fox, A. J., et al. 2017, ApJ, 851, 110
Barlow, R. 2003, in Statistical Problems in Particle Physics, Astrophysics, and
   Cosmology, Proceedings of the PHYSTAT 2003 Conference (Stanford,
  CA: SLAC), 250, http://www.slac.stanford.edu/econf/C030908
Besla, G., Kallivayalil, N., Hernquist, L., et al. 2007, ApJ, 668, 949
Besla, G., Kallivayalil, N., Hernquist, L., et al. 2010, ApJL, 721, L97
Besla, G., Kallivayalil, N., Hernquist, L., et al. 2012, MNRAS, 421, 2109
Bland-Hawthorn, J., & Maloney, P. R. 1999, ApJL, 510, L33
Bland-Hawthorn, J., & Maloney, P. R. 2001, ApJL, 550, L231
Bland-Hawthorn, J., & Maloney, P. R. 2002, in ASP Conf. Ser. 254,
  Extragalactic Gas at Low Redshift, ed. J. S. Mulchaey & J. Stocke (San
  Francisco, CA: ASP), 267
Bland-Hawthorn, J., & Putman, M. E. 2004, in IAU Symp. 217, Recycling
  Intergalactic and Interstellar Matter, ed. P.-A. Duc, J. Braine, & E. Brinks
  (San Francisco, CA: ASP), 12
Bland-Hawthorn, J., Sutherland, R., Agertz, O., & Moore, B. 2007, ApJL,
  670. L109
Brüns, C., Kerp, J., Staveley-Smith, L., et al. 2005, A&A, 432, 45
Cardelli, J. A., Clayton, G. C., & Mathis, J. S. 1989, ApJ, 345, 244
Casetti-Dinescu, D. I., Bidin, C. M., Girard, T. M., et al. 2014, ApJL, 784, L37
Chiappini, C. 2008, in ASP Conf. Ser. 396, Formation and Evolution of Galaxy
  Disks, ed. J. G. Funes & E. M. Corsini (San Francisco, CA: ASP), 113
Diaz, J., & Bekki, K. 2011, MNRAS, 413, 2015
D'Onghia, E., & Fox, A. J. 2016, ARA&A, 54, 363
D'Onghia, E., & Lake, G. 2008, ApJL, 686, L61
Drlica-Wagner, A., Bechtol, K., Allam, S., et al. 2016, ApJL, 833, L5
For, B.-Q., Staveley-Smith, L., & Mcclure-Griffiths, N. M. 2013, ApJ, 764, 74
For, B.-Q., Staveley-Smith, L., Mcclure-Griffiths, N. M., Westmeier, T., &
  Bekki, K. 2016, MNRAS, 461, 892
Fox, A. J., Barger, K. A., Wakker, B. P., et al. 2018, ApJ, 854, 142
Fox, A. J., Wakker, B. P., Barger, K. A., et al. 2014, ApJ, 787, 147
Fox, A. J., Wakker, B. P., Savage, B. D., et al. 2005, ApJ, 630, 332
Gnat, O., & Sternberg, A. 2007, ApJS, 168, 213
Guglielmo, M., Lewis, G. F., & Bland-Hawthorn, J. 2014, MNRAS, 444, 1759
```

```
Haffner, L. M. 2005, in ASP Conf. Ser. 331, Extra-Planar Gas, ed. R. Braun
   (San Francisco, CA: ASP), 25
Haffner, L. M., Reynolds, R. J., & Tufte, S. L. 2001, ApJL, 556, L33
Haffner, L. M., Reynolds, R. J., Tufte, S. L., et al. 2003, ApJ, 149, 405
Hammer, F., Yang, Y. B., Flores, H., Puech, M., & Fouquet, S. 2015, ApJ,
Hill, A. S., Haffner, L. M., & Reynolds, R. J. 2009, ApJ, 703, 1832
Isobe, T., Feigelson, E. D., & Nelson, P. I. 1986, ApJ, 306, 490
Kalberla, P. M. W., Burton, W. B., Hartmann, D., et al. 2005, A&A, 440, 775
Koposov, S. E., Belokurov, V., Torrealba, G., & Evans, N. W. 2015a, ApJ,
Koposov, S. E., Casey, A. R., Belokurov, V., et al. 2015b, ApJ, 811, 62
Koposov, S. E., Walker, M. G., Belokurov, V., et al. 2018, MNRAS, 479, 5343
Lockman, F. J., Benjamin, R. A., Heroux, A. J., & Langston, G. I. 2008, ApJL,
Lu, L., Savage, B. D., & Sembach, K. R. 1994, ApJ, 426, 563
Lu, L., Savage, B. D., Sembach, K. R., et al. 1998, AJ, 115, 162
Madsen, G. J. 2004, PhD thesis, The Univ. Wisconsin
Markwardt, C. B. 2009, in ASP Conf. Ser. 411, Astronomical Data Analysis
   Software and Systems XVIII, ed. D. A. Bohlender, D. Durand, & P. Dowler
   (San Francisco, CA: ASP), 251
McClure-Griffiths, N. M., Madsen, G. J., Gaensler, B. M., McConnell, D., &
   Schnitzeler, D. H. F. M. 2010, ApJ, 725, 275
McClure-Griffiths, N. M., Pisano, D. J., Calabretta, M. R., et al. 2009, ApJS,
```

Mcclure-Griffiths, N. M., Staveley-Smith, L., Lockman, F. J., et al. 2008, ApJ,

Nidever, D. L., Majewski, S. R., Burton, W. B., & Nigra, L. 2010, ApJ,

Nidever, D. L., Majewski, S. R., & Burton, W. B. 2008, ApJ, 679, 432

Oppenheimer, B. D., & Schaye, J. 2013, MNRAS, 434, 1043

181, 398

673, 143

723, 1618

```
Price-Whelan, A. M., Nidever, D. L., Choi, Y., et al. 2019, ApJ, 887, 19
Putman, M. E., Bland-Hawthorn, J., Veilleux, S., et al. 2003, ApJ, 597, 948
Putman, M. E., De Heij, V., Staveley-Smith, L., et al. 2002, AJ, 123, 873
Putman, M. E., Gibson, B. K., Staveley-Smith, L., et al. 1998, Natur, 394, 752
Reynolds, R. J., Tufte, S. L., Haffner, L. M., Jaehnig, K., & Percival, J. W.
  1998, PASA, 15, 14
Richter, P., Fox, A. J., Wakker, B. P., et al. 2018, ApJ, 865, 145
Richter, P., Nuza, S. E., Fox, A. J., et al. 2017, A&A, 607, A48
Ryans, R. S. I., Keenan, F. P., Sembach, K. R., & Davies, R. D. 1997,
           . 289, 986
Sembach, K. R., Howk, J. C., Savage, B. D., & Shull, J. M. 2001, AJ, 121, 992
Smoker, J. V., Fox, A. J., & Keenan, F. P. 2011, MNRAS, 415, 1105
Tepper-García, T., Bland-Hawthorn, J., Pawlowski, M. S., & Fritz, T. K. 2019,
   MNRAS, 488, 918
Tepper-García, T., Bland-Hawthorn, J., & Sutherland, R. S. 2015, ApJ, 813, 94
Thom, C., Putman, M. E., Gibson, B. K., et al. 2006, ApJ, 638, 97
Tufte, S. L. 1997, PhD thesis, The Univ. Wisconsin
Tufte, S. L., Reynolds, R. J., & Haffner, L. M. 1998, ApJ, 504, 773
van Woerden, H., Schwarz, U. J., Peletier, R. F., Wakker, B. P., & Kalberla, P. M. W. 1999, Natur, 400, 138
Venzmer, M. S., Kerp, J., & Kalberla, P. M. W. 2012, A&A, 547, A12
Wakker, B., Howk, C., Schwarz, U., et al. 1996, ApJ, 473, 834
Wakker, B., & van Woerden, H. 1991, A&A, 250, 509
Wakker, B. P., York, D. G., Wilhelm, R., et al. 2008, ApJ, 672, 298
Wannier, P., Wrixon, G., & Wilson, R. 1972, A&A, 18, 224
Weymann, R. J., Vogel, S. N., Veilleux, S., & Epps, H. W. 2001, ApJ,
  561, 559
Winkel, B., Kerp, J., Flöer, L., et al. 2016, A&A, 585, A41
Yang, Y., Hammer, F., Fouquet, S., et al. 2014, MNRAS, 442, 2419
Zhang, L., Casetti-Dinescu, D. I., Moni Bidin, C., et al. 2019, ApJ, 871, 99
```

Pardy, S. A., D'Onghia, E., & Fox, A. J. 2018, ApJ, 857, 101